Wear 574-575 (2025) 206086

Contents lists available at ScienceDirect

Wear

journal homepage: www.elsevier.com/locate/wear

Modelling of tool wear incorporating various feeds in micro-drilling of carbon fibre-reinforced polymer (CFRP) composites

Szilárd Seprős, Balázs Markó, Norbert Geier *

Budapest University of Technology and Economics, Faculty of Mechanical Engineering, Department of Manufacturing Science and Engineering, Műegyetem rkp. 3., Budapest 1111, Hungary

ARTICLE INFO

Keywords:
CFRP
Micro-drilling
Tool wear
Modelling

ABSTRACT

Micro-drilling of carbon fibre-reinforced polymer (CFRP) composites is gaining importance in high-end applications like aerospace to optimize the aerodynamic properties of structural components. However, the micro-drilling process in CFRPs remains challenging, particularly due to the complex and underexplored wear mechanisms of micro-drills. In the case of micro-drilling, the size effect plays a significant role, the ploughing dominancy is considerable and affects the chip formation mechanisms and the tool loading conditions, which are not strictly proportional to the rate of the tool wear. Consequently, the progression and modelling of wear of micro-drills in CFRPs cannot be directly implemented from macro-scale experiences. This study aims to develop a predictive model for flank wear of industrially used uncoated solid carbide micro-drills during CFRP machining. Thousands of holes were drilled to construct a general flank wear model, which was subsequently validated using additional experiments involving hundreds of holes. Tool wear was characterized through digital and scanning electron microscopy, while the influence of feed was analysed through analysis of variances (ANOVA). The developed general model incorporates feed and cutting length to predict micro-drills' flank wear accurately. The proposed model demonstrated high accuracy (maximum 13 % of main absolute percentage error) and robustness, offering a valuable tool for engineers to enhance process planning, maintain machining quality, predict remaining tool lifetime, and improve efficiency in composite micro-drilling operations.

1. Introduction

Nowadays, the use of carbon fibre-reinforced polymer (CFRP) composites has become increasingly widespread, primarily due to their outstanding mechanical properties, such as high strength-to-weight ratio, corrosion resistance, and design flexibility [1]. These composite materials are extensively utilized in advanced industries, including aerospace and energy, where weight reduction and structural performance are critical [2]. While macro-scale machining processes are getting to be a well-explored area [3], the cutting phenomena observed in micro-machining of CFRPs remain more challenging and relatively unexplored [1]. On the one-hand, the machinability of fibrous composites is significantly influenced by fibre orientation, affecting chip removal and surface quality [4]. During drilling fibrous composites, alternating tool engagement with fibres and matrix leads to uneven cutting loads, heat generation, and gradual tool wear due to fibre abrasion and matrix rubbing [5]. The abrasion-related wear issues, the inhomogeneous and anisotropic structures are the key cause of the machining defects, such as interlaminar delamination, burrs, surface cavities and fibre pull-outs [6]. On the other hand, micromachining experiments have already been carried out on a wide range of materials [7,8], with numerous studies on the characteristics of the machining process, in which the phenomenon of the size effect has been explained [9]. For such small material removal, the minimum chip thickness is often comparable to the cutting edge radius, increasing the dominance of the ploughing effect significantly, while increasing the loads and tool wear [10]. To address these challenges together, the knowledge gap is particularly evident despite the growing demand for micro-machining technologies in manufacturing high-precision components, such as polymeric biomedical filters and composite engine nacelles, which enhance aerodynamic performance of CFRP parts [11]. One of the key challenges in machining operations is the monitoring and assessment of tool wear [12–14]. Tool wear directly influences surface quality, dimensional accuracy, and overall process efficiency, especially when machining CFRPs, which are known for their abrasive properties and heterogeneous structure [15,16]. Consequently, this study focuses on the

* Corresponding author.
E-mail address: geier.norbert@gpk.bme.hu (N. Geier).

https://doi.org/10.1016/j.wear.2025.206086
Received 18 December 2024; Received in revised form 27 March 2025; Accepted 17 April 2025
Available online 17 April 2025

investigation of tool wear during the micro-drilling of CFRPs, aiming to contribute to the understanding of wear mechanisms and provide insights for process optimization.

As the challenges of micro machining and drilling of CFRP materials are combined in the micro-drilling of CFRP composites, it becomes essential to evaluate the applicability of existing knowledge and techniques in such an environment. The observed phenomena in the two cases show a close relationship, however, a lower delamination effect and a higher specific tool load were observed in the micro-scaled drilling [17,18]. Two factors that have a significant impact on the machining characteristics, and thus on tool wear, are the geometry of the tool and the applied feed [19,20]. Dogrusadik et al. [21] found that the feed rate has a greater effect on the degree of flank wear than the cutting speed, and they also noted that the use of the backing plate also has a significant effect on flank wear. They have found that using a backing plate results less tool wear, and flank wear decreased with increasing feed in the supporting cases. Wang et al. [22] investigated tool wear of different coated tools (uncoated, diamond coated, AlTiN coated) during drilling of CFRP composite. They found the cutting edge rounding to be the main type of the tool wear. The tool having the diamond coating showed the smallest edge rounding, while the AlTiN coating did not protect the tool due to the oxidation during drilling process. Shyha et al. [23] conducted experiments with a large number of holes and proved that tool wear is mainly influenced by tool geometry and feed rate. They characterized the tool wear by the flank wear, showing the effect of different tool geometries and cutting parameters well. They observed that higher feed, use of uncoated carbide tool and the stepped drill geometry is beneficial condition from the point of view of minimising tool wear.

Tool wear tests were conducted in micromachining experiments, where the effects of machining parameters were investigated and compared with existing micromachining knowledge [24]. Percin et al. [25] examined the micro-drilling of Ti-6Al-4V alloys at different feed rates, cutting speeds, and coolant-lubricant strategies. Their research demonstrated that, particularly during cryogenic drilling, improved tool wear resistance, enhanced surface quality, and reduced machining-induced burr height were achieved. In micromachining experiments, the primary types of tool wear observed were adhesion wear, built-up edge formation, and flank wear [8]. When machining FRP composites, flank wear was identified as the dominant wear form due to the abrasive nature of the material [26,27]. Consequently, the analysis and evaluation of tool wear, while machining abrasive materials is typically based on flank wear or the rounding of the cutting edge. Faraz et al. [28] approached the wear characteristics of abrasive materials by investigating the cutting edge rounding (CER), which indicates the sharpness of the tool. They also observed the correlation between CER and mechanical loads, and between CER and the entry and exit delamination results. Gaugel et al. [17] determined the tool wear by the CER and concluded, that measuring CER is suitable method to characterize tool wear mainly for uncoated tools. They also determined a nearly linear correlation between CER and tool life. Bai et al. [14] developed semi-analytical models to estimate the tool wear processes. They predicted the wear rate of the tool and the half-axes those describe the cutting edge geometry. The validation process showed great results, the prediction errors of the wear rate was less than 25 % and for the average half axis lengths was less than 15 %. However, their robustness analysis showed that changing the two wear coefficients by ±5 % and ±10 % can result in a difference in the prediction of tool wear rates of only 2.78 % and 5.56 %, respectively. Even though CFRP composite micro-drilling experiments have been carried out several times and the main effects have been investigated [21,28], only a few experiments have been carried out with a large number of drilled holes making possible to investigate the wear curve. Investigating tool wear in such cases could reveal the different stages of the wear curve and their characteristics. Modelling and prediction of tool wear is an important element of manufacturing process design, this has been approached in several ways for macro-scaled CFRP machining and may be needed at micro-scaled CFRP machining as well.

Considering the identified gaps and findings in the literature, this study aims to develop an adequate tool wear prediction model with industrial applications in mind. The proposed model aims to accurately predict flank wear, addressing a critical need for enhanced efficiency and reliability in machining operations in carbon fibre-reinforced polymer composites.

2. Experimental setups

The workpiece used in the experiments is a unidirectional (UD) carbon fibre-reinforced vinyl ester matrix composite laminate having $t = 5$ mm nominal thickness. The main material properties were measured in a previous project and are listed in Table 1, where R_m is the tensile strength, τ_m denotes the shear strength, S_m is the Shore D hardness and a_{cN} is the impact strength.

The micro-drilling experiments were carried out on a NCT VHTC-130 LINEAR milling machine centre with dry machining environment, where the chip extraction is provided by Nilfisk GB733 industrial vacuum cleaner. The main specifications of the machine tool are shown in Table 2.

Uncoated solid carbide SECO SD26-0.50–3.20–3R1 micro-drilling tools were used for the experiments having a diameter of ⌀0.5 mm, two cutting edges and 35° helix angle. The run-out of the micro-drills were measured and the tool fixturing was changed iteratively until the run-out was not larger than 50 μm. The tool wear was calculated through digital image processing of images taken by a Dino-Lite AM413T5 digital microscopes after every 30 holes drilled. The experimental setup can be seen in Fig. 1.

In addition to digital microscopy measurements, a Zeiss EVO MA10 scanning electron microscope (SEM) was utilized. This equipment allowed for higher precision in determining actual wear on the tool's rake and flank faces, surface damage, and the cutting edge radius. The measurements were carried out using two different setups. In one arrangement, the objective was to detect the tool's flank face. For this, positioning was achieved with an Olympus SZX16 stereomicroscope at a nominal magnification of 115×. Following the alignment, images of the tools were captured using the SEM at 250x and 1000x magnifications, with an accelerating voltage of 20 kV. The second microscopy setup was focused on detecting the cutting edge radius. This can be achieved by tilting the tool, positioning the cutting edge parallel to the electron beam. The angular position of the tools was adjusted using a Dino-Lite AM413T5 digital microscope. In this case, SEM images were acquired at 1500x and 4000x magnifications, also at 20 kV accelerating voltage. Fig. 2 Illustrates the scanning electron microscope and the fixture aiming to accurately position the micro-drills to capture SEM images perpendicular to the main cutting edge. The applied microscopes and the magnification values used are shown in Table 3.

Trial micro-drilling experiments were conducted in order to determine the process parameters to be investigated. The cutting speed and the feed were varied according to the full factorial design. Therefore, the feed (f) was selected as continuous factor, varied in two levels ($f_1 = 8$ μm, $f_2 = 24$ μm). While the cutting speed and the nominal drilling depth was fixed to $v_c = 50$ m/min and $z = 2$ mm, respectively, the cutting parameters are summarised in Table 4. The experiments were repeated 1000 times in order to get the tool condition significantly change. New micro-drilling tools were used for each experimental setup.

The tool wear (W) was detected parallel with the tool axis and measured three times ($n = 3$), that is transformed to flank wear (VB) according to Eq. (1).

Table 1
Main material properties of the applied UD-CFRP composite [29].

R_m (MPa)	τ_m (MPa)	S_d (1)	a_{cN} (kJ/m^2)
547.9 ± 45.8	21.77 ± 0.70	88.24 ± 0.36	263.17 ± 24.76

Table 2
Specifications of the milling machine.

VHTC-130 5-axis milling machine centre	
Linear axis travel X/Y/Z (mm)	200/180/200
Maximum spindle speed (rpm)	60 000
Maximum cutting feed rate (m/min)	10
Spindle power (kW)	1.2
Maximum tool diameter (mm)	6

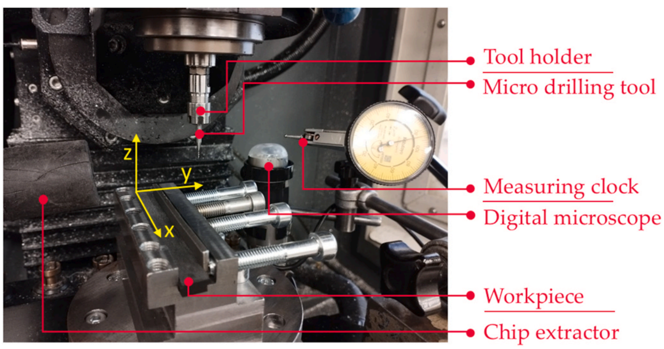

Fig. 1. Micro-drilling experimental setup.

$$VB = \frac{1}{n}\sum_{i=1}^{n}\frac{W_i}{\cos\alpha_o} \tag{1}$$

Where $n = 3$ is the repetition of the W measurements and α_O is the orthogonal clearance angle as illustrated in Fig. 3. Although investigating numerous SEM images of the tool would make possible to observe the exact VB and CER values and their correlation [28,30], these are extremely difficult (difficult tool shape, timely and costly process, etc.) to implement, thus, were not the focus of this study.

3. Results and discussion

3.1. Tool wear progression

Microscopic images captured during the experiments provide clear evidence of progressive tool wear, as shown in Fig. 4. Reflective surfaces, indicative of edge wear, are visible on both the main cutting edge and the chisel edge. The growth in the reflective surface area, corresponding to edge wear, becomes increasingly apparent as the number of drilled holes rises. Additionally, the tool wear is most pronounced at the outer diameter and diminishes toward the inner diameter. This observation aligns with expectations, as the larger tool diameter experiences a higher effective cutting speed, leading to accelerated wear at the periphery [21].

Using scanning electron microscopy (SEM), we obtained more detailed insights into tool wear, enabling a more representative comparison of the tools, as illustrated in Fig. 5. The SEM images clearly show the rounding of tool edges, along with worn and chipped tool surfaces. These high-resolution images provided a more accurate analysis of the cutting edge radius (CER), allowing us to refine our understanding of the flank wear process. Fig. 5a shows the micro-drill tool geometry before cutting. The primary clearance surface is smooth and flat, while the CER is uniform and small compared to the CER of the worn tools. Fig. 5b and c show extended edge rounding having uniform and smooth surfaces, which suggest that the tool wear is dominated by the abrasive wear, as it was expected due to the abrasive nature of the carbon fibre reinforcements [31]. Chipping of the main cutting edge was also observed in Fig. 5b, which geometry is also smooth but its characterising geometry does not follow the geometry of the main cutting edge (see the yellow dashed lines in the figure). Edge chipping when micro-drilling CFRPs was also observed by Kim et al. [32]. Edge chipping will result in an even more difficult-to-control process because the chip cross section will be significantly different to the expected rectangular shape that may results in more energy to fracture the chip. If the edge chipping gets comparable in size to the length of the main cutting edge, the micro-drilling process probably cannot be considered be sustainable or green; however, this needs to be proved in the future by dedicated experiments.

The SEM images provided an essential validation of the W values measured using the experimental microscope. They confirmed that the reflective surface corresponds accurately to the worn section of the tool. For this validation, only images of the tool taken before and after micro-drilling were available. Nevertheless, these images allowed the measured W values to be effectively correlated with the flank wear, as illustrated in Fig. 6.

Based on the SEM images, the CER values were not measured because the excessive displacement of the cutting edge and the rounding by the cutting edge corner (both due to tool wear) did not allow to take images of the tools at the specified angular position even with the application of the dedicated fixture (Fig. 2b). However, it could be seen from the images taken of the tools that the CER geometry is roughly uniform and smooth, therefore, the conversion of the original W values to the amount of flank wear VB can be given by a trigonometrical function based on the clearance angle, as was expressed by Eq. (1).

The flank wear values depicted from the evaluated data is shown in Fig. 7 as a function of the cutting length for the feed level values of 8 μm and 24 μm. The graph values for the feed levels are distinct from each other, but their shape is similar. Considering that the larger the feed, the larger the chip cross-section, thus the larger the cutting force; a larger tool wear was expected in the case of larger feed applied. However, the highest feed level is typically associated with the lowest edge wear value according to the results shown in Fig. 7. This phenomenon can be attributed mostly with the size effect. Lower feeds during micro-drilling results in smaller uncut chip thickness. When the uncut chip thickness becomes comparable to the cutting edge radius (CER), i.e., the uncut chip thickness is smaller than the minimal chip thickness, ploughing is getting dominating the chip formation mechanisms. In micro-drilling, an increase in the CER further enhances ploughing-dominated chip formation, leading to higher tool loads and, consequently, an increased tool wear rate. On the other hand, considering that the nominal carbon fibre diameter (7–8 μm) is comparable to the applied smallest feed (8 μm), an improper chip removal could arise in this case resulting in larger tool wear speed. In addition, the larger the feed, the smaller the time the tool contacting with the composite; thus, the machining-induced cutting temperature and the tool wear is expected to be smaller.

Some regions of the flank wear diagram can be compared with the stages of the typical wear curve. The wear process up to the first ~600 mm of the total cutting length comparable to the initial wear stage of the typical wear curve, while the further phase reveals a phase of steady wear stage. The wear-out stage cannot be determined exactly from Fig. 7. The curves associated with the feed levels show a similar character and values in the initial stage, but in the steady wear stage they take a visibly different slope. This characteristic was investigated by analysis of variances (ANOVA), where we examined the significance of the effect of different feed levels on the flank wear at the (i) initial wear stage and the (ii) steady wear stage. The ANOVA were carried out at 6-6 different measurement points of the stages. The results at the initial wear stage are summarised in Table 5, showing the F- and P-values of the statistics for each feed level.

Based on the ANOVA results, the effect of the feed is mostly not significant at the initial wear stage. This insignificance may be due to the rapid tool wear speed resulted relatively large deviations of measured values. The ANOVA results at the steady wear stage are summarised in Table 6, showing the F- and P-values of the statistics for each feed level.

Based on the ANOVA results, the effect of the feed is significant at the steady wear stage, as expected because the feed has a direct influence on

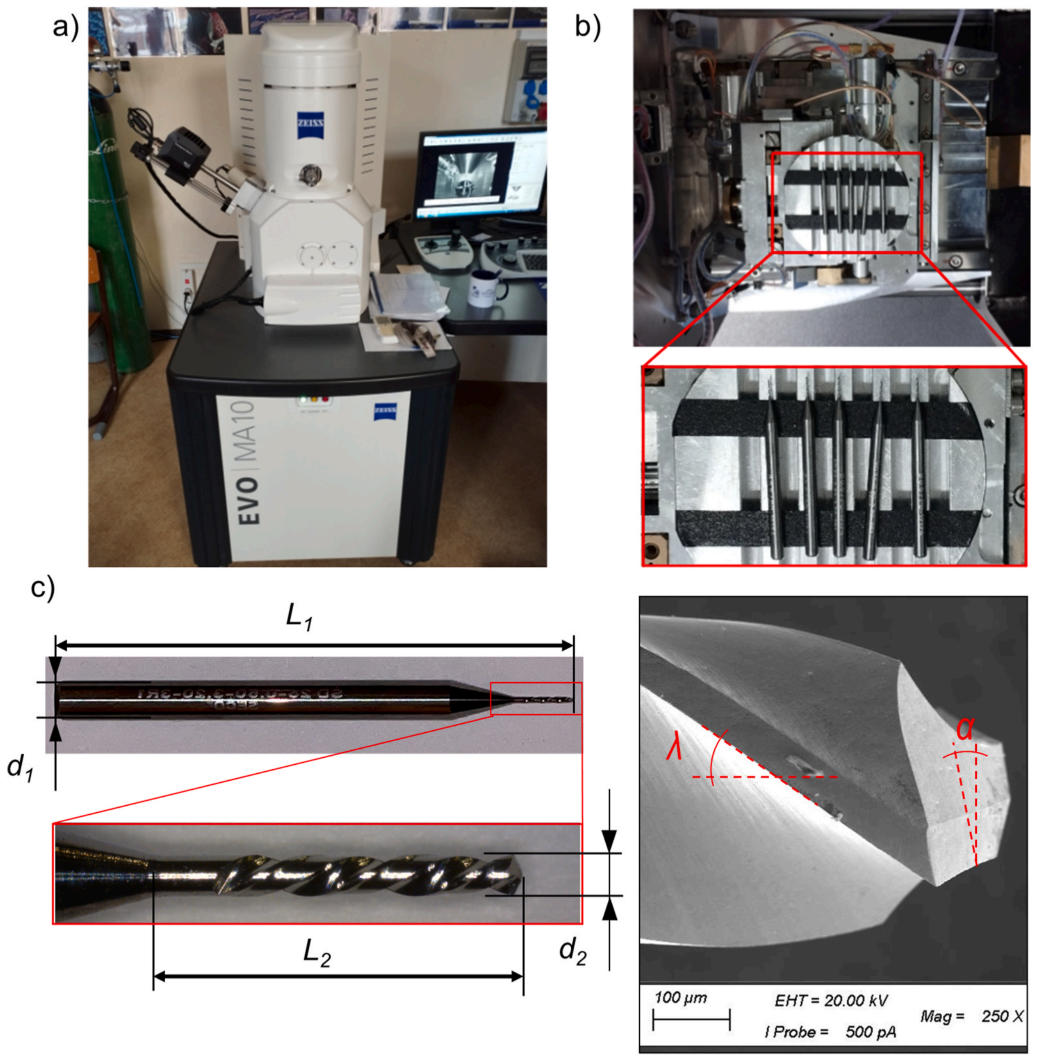

d_1	d_2	L_1	L_2	Point angle	Helix angle	Relief angle	Number of cutting edges
3 mm	0.5 mm	38 mm	4 mm	130°	35°	10°	2

Fig. 2. (a) Zeiss EVO MA10 scanning electron microscope (SEM) and (b) positioning of the micro-drilling tools in the working area of the SEM using a fixture, (c) the geometrical parameters of the micro-drilling tool.

Table 3
The applied microscopes and the used magnifications.

Manufacturer	Type	Applied magnification
Zeiss	EVO MA10 scanning electron microscope	250; 1000; 1500; 4000
Olympus	SZX16 stereomicroscope	115
Dino-Lite	AM413T5 digital microscope	200

Table 4
The applied cutting parameters.

Tool diameter	Cutting speed	Drilling depth	Feed	Number of holes
d (mm)	v_c (m/min)	*z* (mm)	*f* (µm)	*n* (1)
0.5	50	2	8; 24	1000

the chip cross section. It must be also highlighted, that the tool wear measuring accuracy is better if the tool wear is accelerated. Therefore, the measuring accuracy of small tool wear (i.e., tool wear at the initial stage) is smaller than in the following stages. The main effect plots are shown in Fig. 8. As shown in Fig. 8a, the effect of the feed seems to be not consistent, and, in some cases, the effect appears to be opposing. This concludes that the interaction of feed and the cutting length is considerable at the initial wear stage. In addition, the large P-values (>0.05) in Table 5 suggest that the variances are too large compared to the differences of the means. However, at the end of the initial wear stage, the wear values for the two feeds are more distinct, in certain cases the effect of the feed can be considered significant. As depicted in Fig. 8b, the effect of the feed is significant in the steady wear stage, as the confidence intervals are significantly smaller compared with the deviations of the means (expected values of tool wear). This is proved also by the calculated small P-values shown in Table 6. In addition, the interaction of the feed and cutting length is not considerable. Based on the ANOVA results, the lowest flank wear values were found at the higher feed level. The

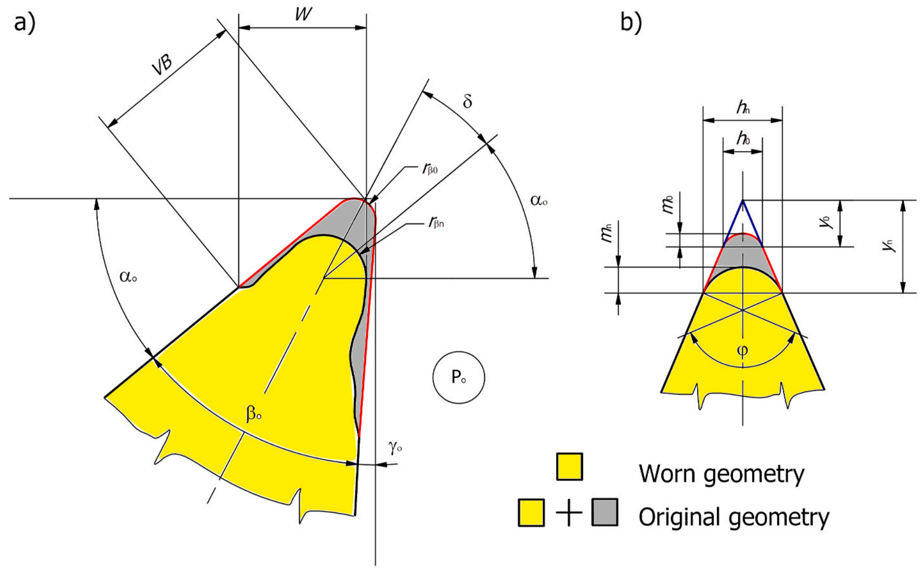

Fig. 3. A schematic drawing of the edge of the micro-drilling tool in the (a) orthogonal plane and illustration of the (b) theoretical geometric data, where α_0 is the orthogonal clearance angle, β_0 is the orthogonal wedge angle, γ_0 is the orthogonal rake angle, r_β is the cutting edge radius (also known as CER).

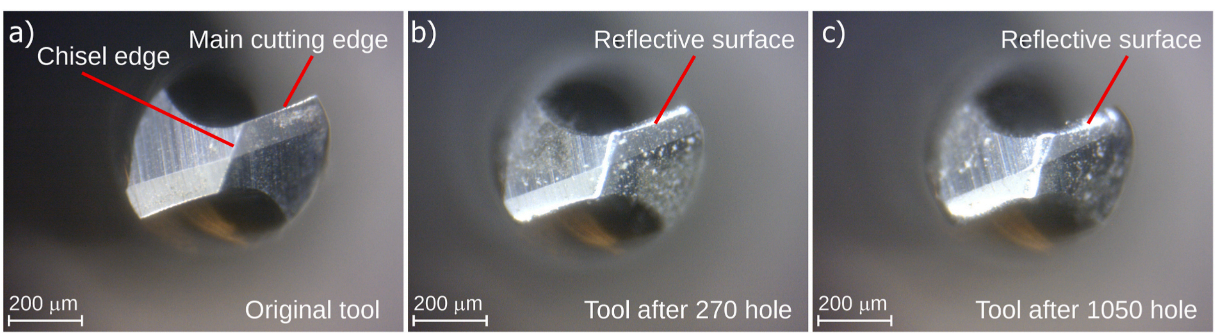

Fig. 4. Progress of tool wear of the applied micro-drill at feed of 24 μm, i.e., a) the starting tool geometry, b) tool geometry after 270 holes were drilled, and c) tool geometry after 1050 holes were drilled.

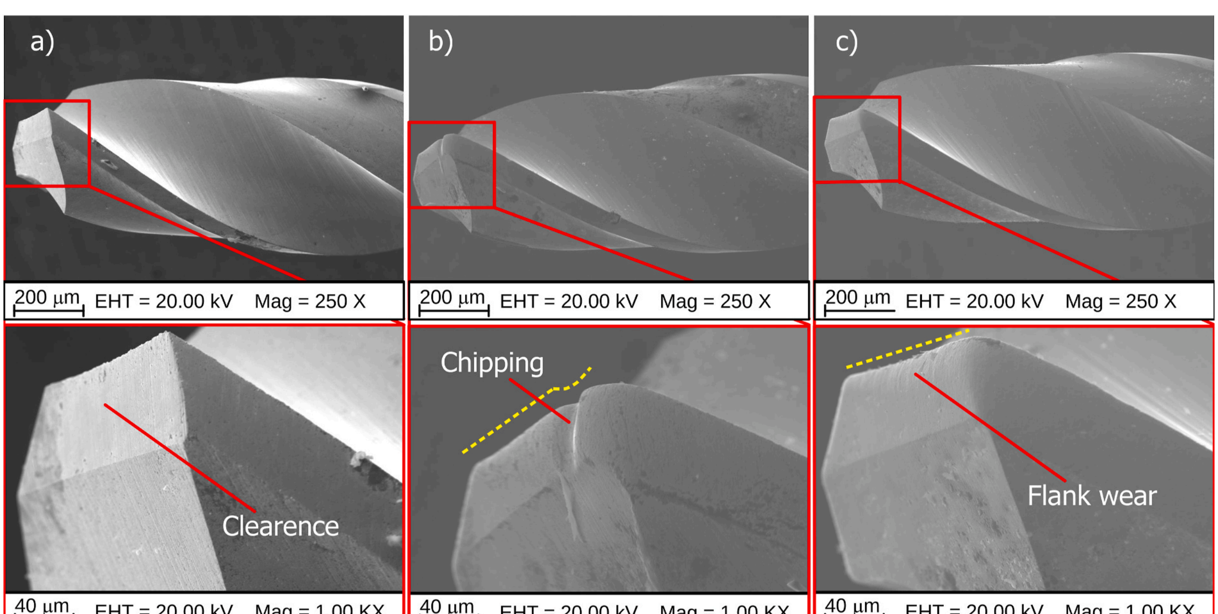

Fig. 5. Scanning electron microscopic images of the flank surface of the micro-drills: a) original tool geometry before cutting, b) tool geometry after 1050 holes at feed of 8 μm, c) tool geometry after 1050 holes at feed of 24 μm.

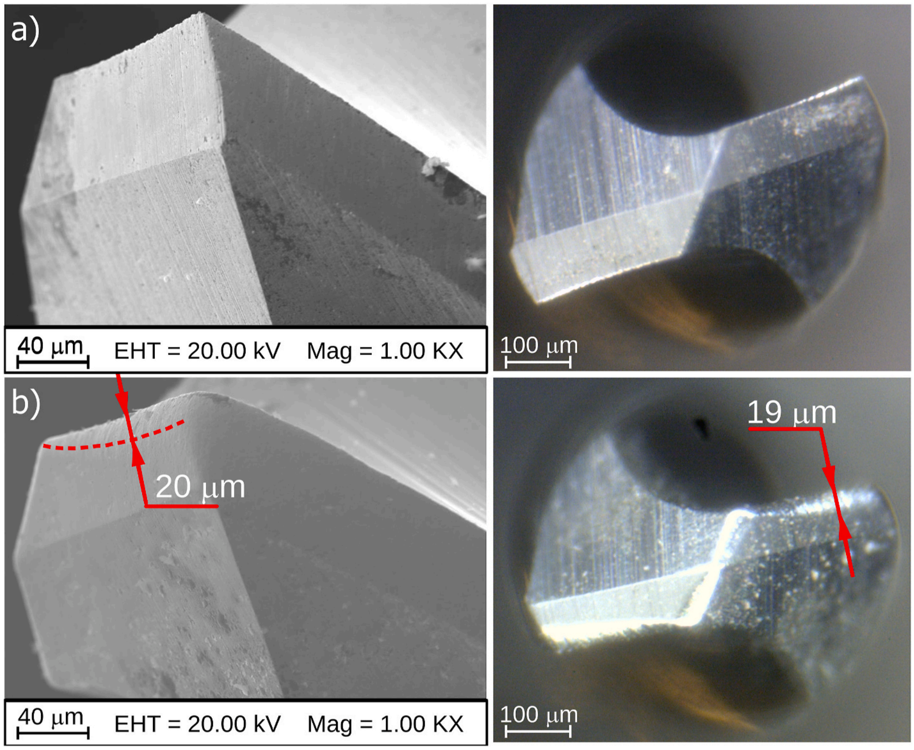

Fig. 6. Scanning electron microscopic and optical images of the micro-drills: a) sharp edges of the micro-drill prior to the experiments, b) drilling-induced tool wear on the flank surface of the micro-drill after machining 1050 holes.

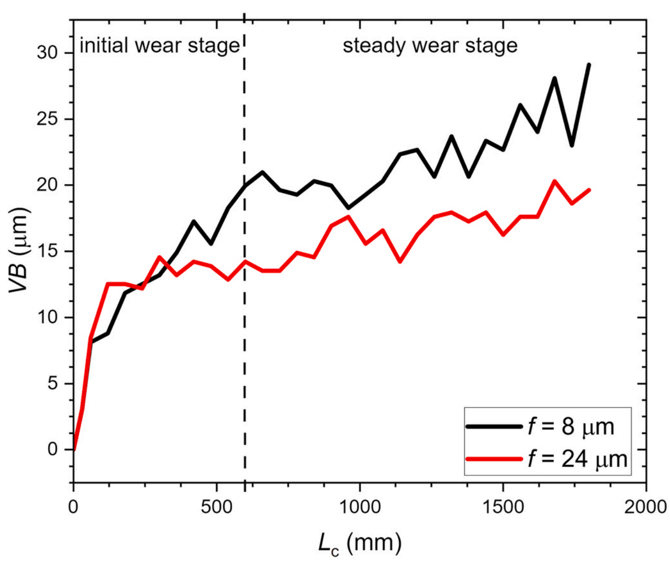

Fig. 7. Flank wear propagation of the micro-drills at different feed levels.

Table 5
ANOVA table for initial wear stage, where the bold P-values indicate that the influence of the feed on the tool wear is significant at the significance level of α = 0.05

Cutting length (mm)	Source	DF	Adj SS	Adj MS	R^2 (%)	F-value	P-value
30	Group	1	0.1718	0.1718	20.0	1.00	0.374
	Error	4	0.6874	0.1718			
	Total	5	0.8592				
120	Group	1	20.79	20.794	60.2	6.05	0.070
	Error	4	13.75	3.437			
	Total	5	34.54				
240	Group	1	0.1718	0.1718	1.89	0.08	0.795
	Error	4	8.9361	2.2340			
	Total	5	9.1080				
360	Group	1	24.746	24.746	85.71	24.00	**0.008**
	Error	4	4.124	1.031			
	Total	5	28.817				
480	Group	1	4.296	4.2962	55.56	5.00	0.089
	Error	4	3.437	0.8592			
	Total	5	7.733				
600	Group	1	49.6642	49.6642	98.63	289.00	**0.000**
	Error	4	0.6874	0.1718			
	Total	5	50.3516				

same trend can be found over the whole micro-drilled range which proves the significancy of the feed on the tool wear, proving indirectly the goodness of the applied measuring setup.

3.2. Tool wear modelling

Based on the observed flank wear progress (Fig. 7), the flank wear was modelled using mathematical models. Three models (linear, power-law based, third-order approximate) were developed to meet multiple (and often contradictory) requirements i.e., being simple, easy to derivate, fit well, short, easy to interpret, fast to calculate, follow mechanistic rules *etc*. The most common approximation is the linear regression [17,33], therefore, we modelled the VB using a linear model first, as expressed by Eq. (2).

$$VB_{lin}(L_c) = C_1 \cdot L_c + C_2 \tag{2}$$

Where VB_{lin} is the linear model of the flank wear, L_c denotes the cutting length and C_i are linear regression coefficients. The regression coefficients are listed in Table 7.

The use of a third-order polynomial function is useful for modelling flank wear, as it can fit the theoretical wear curve quite closely [34]. In addition, a well-defined third-order function could be used for extrapolation beyond the experimental range, depending on the quality and

Table 6
ANOVA table for steady wear stage, where the bold P-values indicate that the influence of the feed on the tool wear is significant at the significance level of α = 0.05

Cutting length (mm)	Source	DF	Adj SS	Adj MS	R^2 (%)	F-value	P-value
600	Group	1	49.6642	49.6642	98.63	289.00	**0.000**
	Error	4	0.6874	0.1718			
	Total	5	50.3516				
840	Group	1	49.664	49.664	84.75	22.23	**0.009**
	Error	4	8.936	2.234			
	Total	5	58.600				
1080	Group	1	20.7937	20.7937	96.80	121.00	**0.000**
	Error	4	0.6874	0.1718			
	Total	5	21.4811				
1320	Group	1	49.664	49.664	86.79	26.27	**0.007**
	Error	4	7.561	1.890			
	Total	5	57.226				
1560	Group	1	107.405	107.405	98.74	312.50	**0.000**
	Error	4	1.375	0.344			
	Total	5	108.780				
1800	Group	1	134.73	134.729	90.74	39.20	**0.003**
	Error	4	13.75	3.437			
	Total	5	148.48				

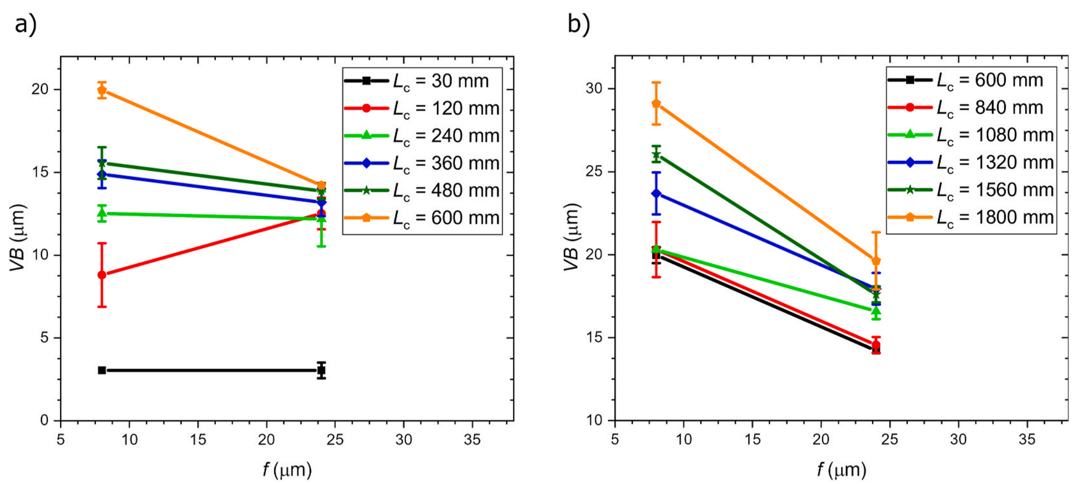

Fig. 8. Main effect of the feed on the flank wear at the a) initial wear stage and b) steady wear stage.

Table 7
List of regression coefficients (C_i) for the VB models developed.

f (µm)	VB_{lin}		VB_{th}				VB_{pow}	
	C_1	C_2	C_3	C_4	C_5	C_6	C_7	C_8
8	10.39	0.0095	4.603	0.0407	−3.6E-5	1.14E-8	2.2192	0.3242
24	10.31	0.0053	7.085	0.0237	−2.2E-5	7.2E-9	3.9276	0.2050

quantity of the fitting data and the goodness of fit. Therefore, a third-order polynomial model is developed second, as expressed by Eq. (3).

$$VB_{th}(L_c) = C_3 \cdot L_c^{\,3} + C_4 \cdot L_c^{\,2} + C_5 \cdot L_c + C_6 \quad (3)$$

A power-law function was also applied to model the flank wear progress, which shape can approximate the initial and the steady wear stages of the theoretical wear curve with a close fit. Although this function cannot represent the progressive stage of the wear curve, it is often acceptable because the modelling of the progressive wear state is not in the focus of industrial interest. The applied power-law model is expressed by Eq. (4).

$$VB_{pow}(L_c) = C_7 \cdot L_c^{\,C_8} \quad (4)$$

The three developed flank wear models are shown in Fig. 9 for the two applied feed values.

Based on Fig. 9, the third-degree and power models provide a better fit to the measured values, than the linear model. The power model shows the best fit, as it can describe well the initial and steady wear stages that were observed, which roughly consists of a degressive and a steady stage. The third-degree model has also a good fit and is able to describe the progressive part of the wear curve, which could be more accurate for an experiment with a larger number of drilled holes. The developed models have been evaluated with the mean absolute percentage errors (MAPE). The MAPE values of the VB models are summarised in Table 8.

As shown in Table 8, the linear model gives the highest MAPE values, and the power model gives the lowest. This difference in the goodness of predictions is proportional to the number of regression coefficients of these models. The MAPE are the highest at the initial stage, due to the accelerated wear process in the initial stage, which led to uncertain results. The steady wear stage shows clearly lower MAPE values, as

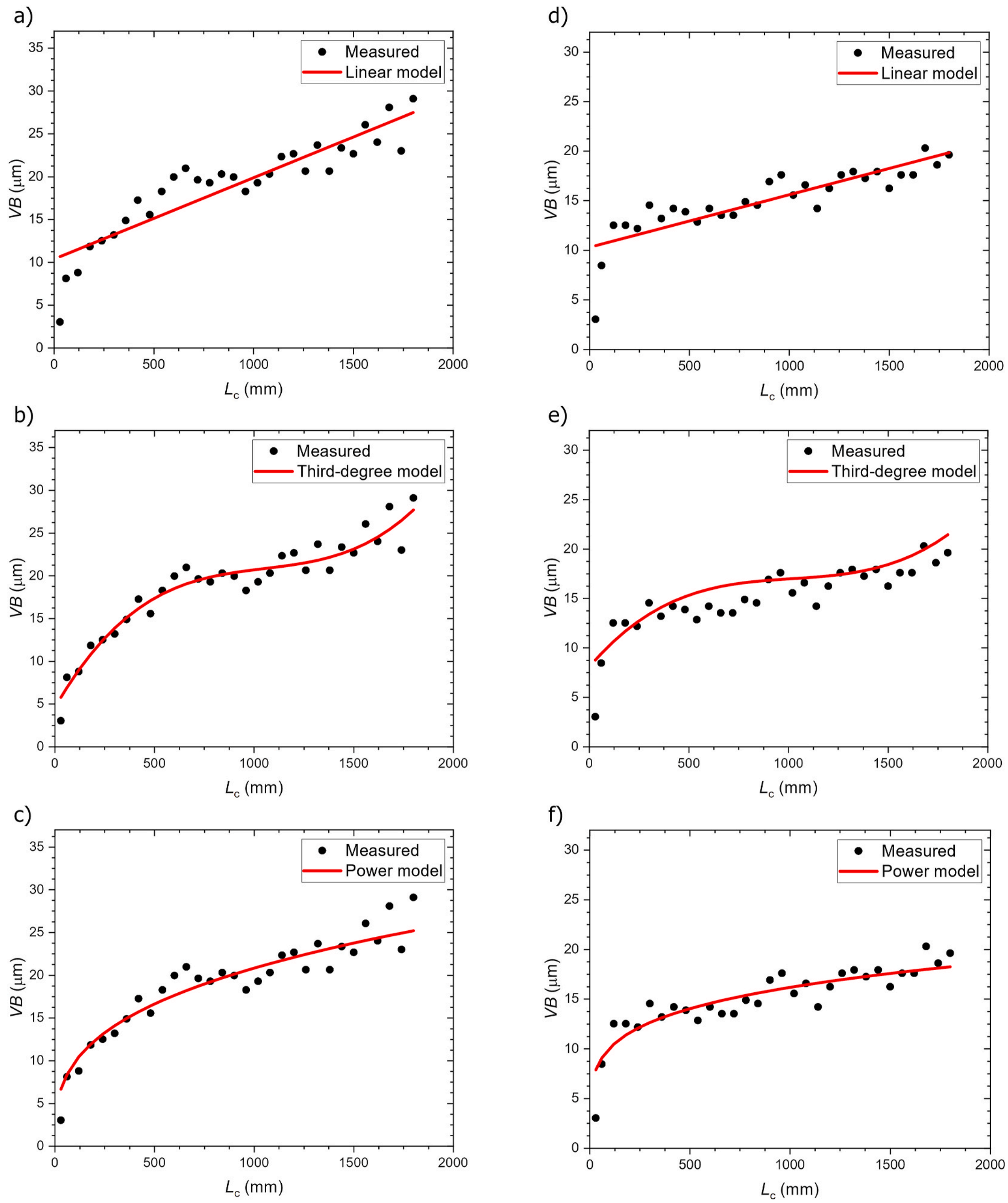

Fig. 9. Illustration of the developed tool wear models: a) linear model for $f = 8$ µm, b) third-degree model for $f = 8$ µm, c) power model for $f = 8$ µm, d) linear model for $f = 24$ µm, e) third-degree model for $f = 24$ µm and f) power model for $f = 24$ µm.

Table 8
Mean absolute percentage errors (MAPE) of the developed models in each feed level.

Wear region	$f = 8$ µm			$f = 24$ µm		
	VB_{lin}	VB_{th}	VB_{pow}	VB_{lin}	VB_{th}	VB_{pow}
Initial wear stage	33.99 %	10.20 %	6.94 %	31.37 %	19.73 %	10.40 %
Steady wear stage	7.75 %	5.80 %	5.95 %	5.24 %	6.43 %	5.71 %
Full drilled range	17.37 %	7.41 %	6.31 %	14.82 %	11.30 %	7.43 %

expected due to the more stable process characteristics.

A general flank wear model that is incorporating not only the cutting length (L_c) but the feed (f) also, was developed based on nonlinear regression using the Gauss-Newton iterative algorithm [35] with a maximum iteration number (n_{it}) of 200 and tolerance of 0.00001. Equation (5) shows the general form of the general model, where A, B and C regression coefficients were calculated to 5.10229, 3.01516 and 1.50895, respectively, using $n_{it} = 4$ iterations starting from (10, 10, 10) starting values.

$$VB(L_c, f) = A - B \cdot (\ln(f - C) - \ln L_c) \tag{5}$$

The general models for the two feeds with the measured data are shown in Fig. 10. The mean absolute percentage errors (MAPE) were 11.67 % and 7.12 % for the smaller and higher feeds, respectively. These relatively small MAPE values indicate the accuracy and robustness of the general VB model. The MAPE values for the general model are lower the

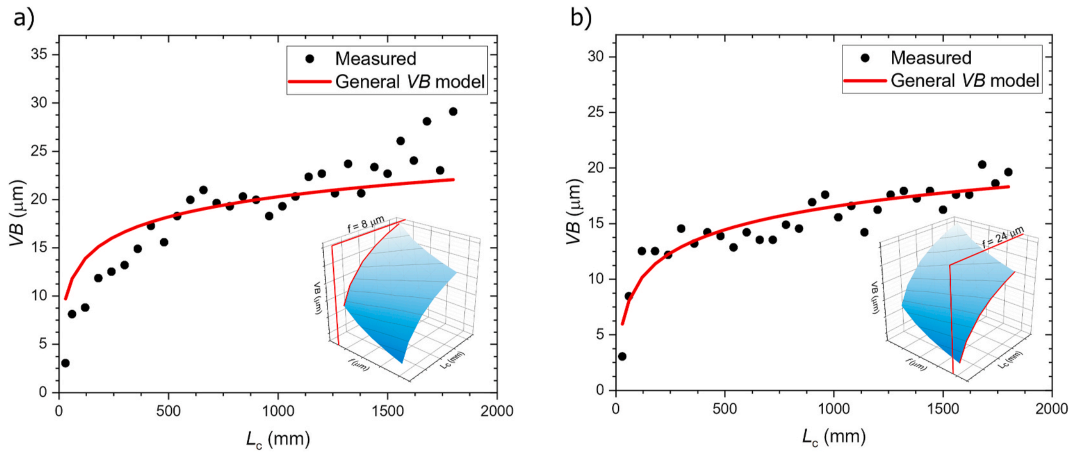

Fig. 10. Flank wear propagation of the micro-drills and general VB model, when the feed was set to a) $f = 8$ μm and b) $f = 24$ μm.

MAPE values of the linear models and are also very close, but higher than the third-degree or power models. This suggests the accuracy of the general model. The graphs show a visibly good fit for the smaller and the higher feeds too, obviously not as good as the separately calculated models. It can be seen that the general model developed from the experimental values is promising, therefore, it should be tested and validated on a separate experimental data set to prove its robustness, as presented in the next section.

3.3. Validation, discussion and outlook

Although the developed general VB model demonstrates a strong fit to the experimental results, its robustness was further validated using new experimental data. Additional experiments were conducted under the same conditions outlined in Section 2. The cutting speed and nominal drilling depth were maintained at $v_c = 50$ m/min and $z = 2$ mm, respectively, while the feed was set to $f = 16$ μm, falling between the original feed values. A total number of 1050 micro holes were drilled for this validation purpose and the toll geometry was captured and evaluated after every 30 holes. The propagation of flank wear observed on the micro-drill, along with the general VB model predictions, is presented in Fig. 11a, while the residual plot is shown in Fig. 11b. The residual plot illustrates the deviations of the measured VB values from the predictions of the proposed general VB model. The minimal residual observed is 0.047 μm (0.25 % relative error), the maximal residual is 6.07 μm (29.89 %), and the mean absolute residual is 1.48 μm (8.2 %). Notably, 90 % of the residuals are below 4.2 μm, demonstrating the robustness and reliability of the model for predicting flank wear during the micro-drilling of CFRP composites.

The quality of the model fit is characterized by a MAPE of 12.21 %, highlighting its reliability and robustness, the MAPE results of the proposed model are shown in Table 9, comparing the accuracy of the model at different feeds. These results confirm that the model is particularly suited for predictive tool change management in industrial settings within the feed range of 8 μm–24 μm.

In practical applications, cutting tools are often replaced well before reaching the critical tool wear criteria to ensure the quality of machined features, particularly geometric accuracy and surface finish. This conservative approach is usually necessitated by the challenges of implementing real-time or reliable indirect measurement methods for tool wear in industrial environments. However, this practice may lead to premature tool disposal, reducing the overall sustainability and cost-efficiency of the process. By accurately predicting flank wear, the proposed VB model has the potential to extend the practical tool life while maintaining machining quality.

Table 9
Mean absolute percentage errors (MAPE) of the general model in each feed level.

Wear region	f (μm)		
	8	*16*	*24*
Initial wear stage	21.46 %	19.13 %	16.43 %
Steady wear stage	6.01 %	8.20 %	1.73 %
Full drilled range	11.67 %	12.21 %	7.12 %

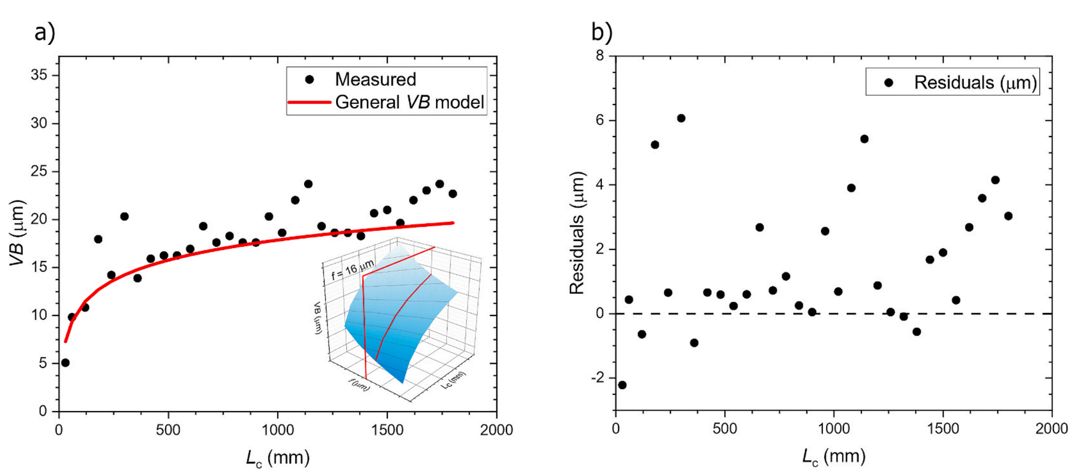

Fig. 11. a) Flank wear propagation of the micro-drill during the validation experiments ($f = 16$ μm) and general VB model, b) residual plot.

While the general VB model shows strong predictive capability, several limitations should be addressed in future research. Firstly, the current model was developed and validated under specific cutting conditions, including fixed cutting speed and a limited feed range. Although the analysed conditions are industrially accepted, their applicability to a broader range of machining parameters, such as high-speed drilling or varying feed rates in a broader range, needs to be further investigated. Secondly, the model does not account for the influence of tool geometry, material properties or coatings, which can significantly affect tool wear behaviour in micro-drilling. Future work could focus on integrating such parameters to enhance the model's generalizability.

Additionally, the model primarily addresses tool flank wear and does not explicitly consider other types of wear mechanisms, such as edge chipping (Fig. 5b), which can also impact tool performance and machining quality. Expanding the model to include these phenomena could provide a more comprehensive tool wear prediction framework. Finally, the current model assumes uniform material properties in the CFRP composite along the unidirectional fibres, while inhomogeneities and anisotropies of non-unidirectional CFRPs can cause localized deviations in tool wear. Incorporating advanced material characterization techniques or finite element modelling could help address this limitation.

Although the assessment of the quality of drilled holes was not the primary focus of this work, we captured images of each machined hole and analysed them to evaluate the cutting process through the quality of the machined geometries. The images were taken using a Keyence VR-5200 profilometer (with a nominal magnification of 80× and a display resolution of 0.1 μm) and were evaluated through digital image processing according to Pereszlai et al. [36]. Representative processed hole images are presented in Fig. 12. To characterize the holes, we used the burr-free factor [37] ($F_{bf} = A_{bf}/A_{nom}$, where A_{bf} denotes the white area in Fig. 12, ie., burr free area, and A_{nom} denotes the nominal hole area) as a key metric, i.e., the larger the F_{bf}, the better the hole quality. Given that more than 3000 holes were drilled, image processing was automated in a MATLAB environment. The F_{bf} of the initial holes ranged between 0.96 and 0.99, while for the last few holes, it typically ranged between 0.88 and 0.92. The continuous decrease in the burr-free area factor was expected due to tool wear, and its trend was closely linear, allowing us to indirectly assess the tool wear progression.

Although delamination is a major challenge in conventional-sized machining of CFRP composites, it was not observed even at progressed tool wear states in micro-sized drilling. Since our experiments involved blind holes, exit delamination was not a concern. However, entry quality of the holes were evaluated using 3D morphological images obtained with the Keyence profilometer. The analysis did not reveal any visible delamination, as it was expected due to the lower cutting force than the interlaminar strength of the composite [38].

Future investigations should also explore the integration of real-time data acquisition systems, such as vibration, acoustic emission, or cutting force monitoring, to enhance the predictive accuracy of the model and facilitate its implementation in smart manufacturing environments. These advancements will help bridge the gap between academic research and industrial application, enabling more sustainable and efficient micro-drilling for CFRP composites.

4. Conclusions

This study focused on modelling tool wear during the micro-drilling of carbon fibre-reinforced polymer (CFRP) composites. The developed model incorporates feed and cutting length to predict the flank wear (VB) of micro-drills accurately. Its reliability was validated against additional experimental data, demonstrating its effectiveness in capturing the wear behaviour. Based on the findings of this research, the

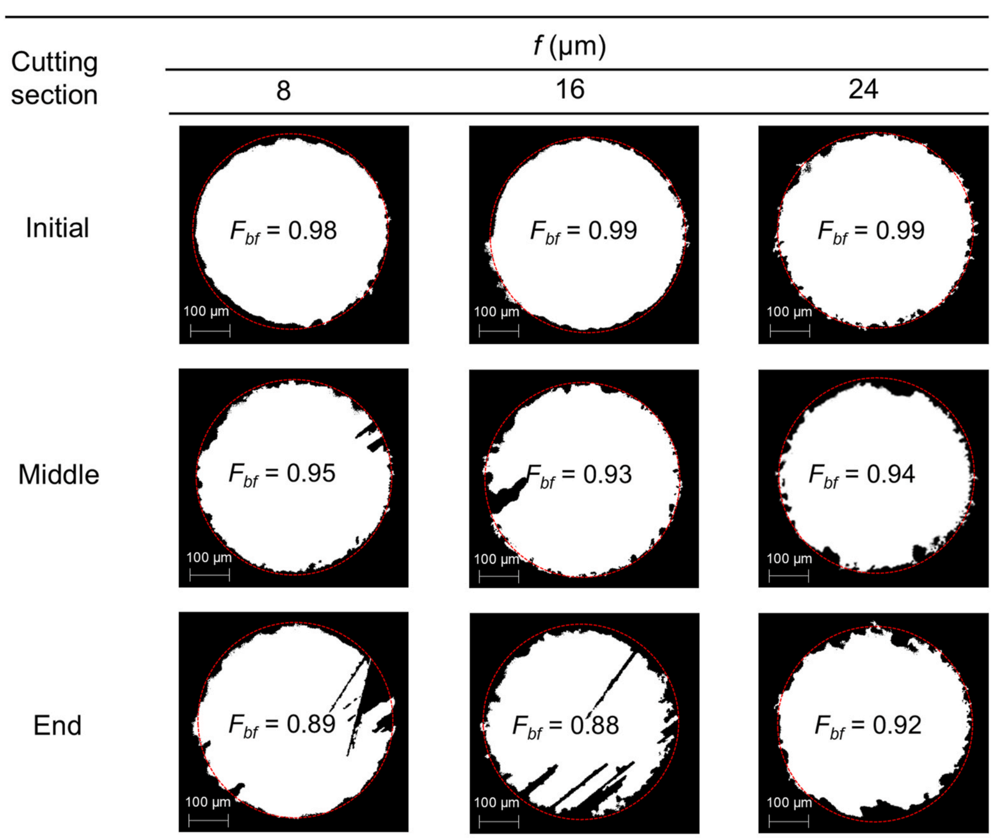

Fig. 12. Representative hole images at different feeds and different experimental stages, presenting the F_{bf} values and the nominal hole diameter.

following conclusions can be drawn.

- We observed through scanning electron microscopy of worn micro-drills large cutting edge rounding and flank wear (18 μm–24 μm) having uniform and smooth surfaces, proving the dominancy of the abrasive wear. Chipping of the main cutting edge was also observed at the largest applied feed (24 μm), which chipped geometry surface is also smooth, but its characterising geometry does not follow the geometry of the main cutting edge, making the tool wear modelling even more challenging.
- Analysis of variance (ANOVA) results show that the influence of the feed on the flank wear is significant in the steady wear stage; however, its significancy in the initial wear stage is not consequent. In the steady wear stage, the larger the feed, the smaller the flank wear in terms of cutting length. In addition, the interaction of the feed and the cutting length is not considerable in the steady wear stage.
- A general flank wear model was developed incorporating the cutting length and the feed, based on nonlinear regression using the Gauss-Newton iterative algorithm with a maximum iteration number of 200 and tolerance of 0.00001. The developed general flank wear model shows a good fit to the experimental results. The accuracy and robustness of the general model was tested through addition experiments. The mean absolute percentage errors (MAPE) are 13.48 %, 12.21 % and 11.92 % for the feeds of 8 μm, 16 μm and 24 μm, respectively.
- While the general flank wear model shows strong predictive capability, several limitations should be addressed in future research, such as (i) extend the models applicability to a broader range of machining parameters, such as high-speed drilling and varying feed rates in a broader range, (ii) account for the influence of tool geometry, material properties or coatings, which can significantly affect tool wear behaviour in micro-drilling, (iii) explicitly consider other types of wear mechanisms, such as edge chipping, which can also impact tool performance and machining quality, (iv) incorporate inhomogeneities and anisotropies of non-unidirectional CFRPs, (v) integration of real-time data acquisition systems, such as vibration, acoustic emission, or cutting force monitoring, to enhance the predictive accuracy of the model and facilitate its implementation in smart manufacturing environments.

CRediT authorship contribution statement

Szilárd Seprős: Writing – original draft, Visualization, Methodology, Investigation, Formal analysis, Conceptualization. **Balázs Markó:** Writing – original draft, Visualization, Methodology, Formal analysis. **Norbert Geier:** Writing – original draft, Methodology, Investigation, Conceptualization.

Consent to participate

Not applicable.

Availability of data and material

The data that support the findings of this study are available from the corresponding author, upon reasonable request.

Code availability

Not applicable.

Ethics approval

Not applicable.

Consent for publication

Not applicable.

Declaration of generative AI and AI-assisted technologies in the writing process

During the preparation of this work the authors used ChatGPT in order to improve the English texting. After using this tool, the authors reviewed and edited the content as needed and take full responsibility for the content of the publication.

Funding

Not applicable.

Declaration of competing interest

The authors declare that they have no known competing financial interests or personal relationships that could have appeared to influence the work reported in this paper.

Acknowledgements

This research was partly supported by the János Bolyai Research Scholarship of the Hungarian Academy of Sciences No. BO/00508/22/6 and has been implemented with the support provided by the Ministry of Culture and Innovation of Hungary from the National Research, Development and Innovation Fund, financed under the EKÖP-24-1-BME-173, EKÖP-24-2-BME-184 and EKÖP-24-4-II-BME-157 funding scheme. The authors acknowledge the support of Endre János Maróti in the experimental work.

Data availability

Data will be made available on request.

References

[1] N. Geier, et al., A critical review on mechanical micro-drilling of glass and carbon fibre reinforced polymer (GFRP and CFRP) composites, Compos. B Eng. 254 (Apr. 2023) 110589, https://doi.org/10.1016/j.compositesb.2023.110589.

[2] V. Mathiyazhagan, A. Meena, Machining-induced damages in the drilling of CFRP under dry and cryogenic environments, Int. J. Adv. Manuf. Technol. 134 (1) (Sep. 2024) 605–626, https://doi.org/10.1007/s00170-024-14120-7.

[3] J. Xu, et al., A critical review addressing drilling-induced damage of CFRP composites, Compos. Struct. 294 (Aug. 2022) 115594, https://doi.org/10.1016/j.compstruct.2022.115594.

[4] J. Xu, J.P. Davim, Machining of fibrous composites: recent advances and future perspectives, in: J.P. Davim (Ed.), Mechanical and Industrial Engineering: Historical Aspects and Future Directions, Springer International Publishing, Cham, 2022, pp. 161–177, https://doi.org/10.1007/978-3-030-90487-6_6.

[5] J. Xu, C. Li, M. Chen, M. El Mansori, J. Paulo Davim, On the analysis of temperatures, surface morphologies and tool wear in drilling CFRP/Ti6Al4V stacks under different cutting sequence strategies, Compos. Struct. 234 (Feb. 2020) 111708, https://doi.org/10.1016/j.compstruct.2019.111708.

[6] J. Xu, T. Lin, J.P. Davim, M. Chen, M. El Mansori, Wear behavior of special tools in the drilling of CFRP composite laminates, Wear 476 (Jul. 2021) 203738, https://doi.org/10.1016/j.wear.2021.203738.

[7] İ. Ucun, K. Aslantas, F. Bedir, An experimental investigation of the effect of coating material on tool wear in micro milling of Inconel 718 super alloy, Wear 300 (1) (Mar. 2013) 8–19, https://doi.org/10.1016/j.wear.2013.01.103.

[8] A. Balcı, A. Çiçek, N. Uçak, K. Aslantas, Investigation of the effects of heat treatment and hot isostatic pressing in micro-drilling of Ti6Al4V alloy fabricated by laser powder bed fusion, Precis. Eng. 91 (Dec. 2024) 617–631, https://doi.org/10.1016/j.precisioneng.2024.10.016.

[9] M. Hasan, J. Zhao, Z. Jiang, A review of modern advancements in micro drilling techniques, J. Manuf. Process. 29 (Oct. 2017) 343–375, https://doi.org/10.1016/j.jmapro.2017.08.006.

[10] U. Karakılınç, B. Ergene, B. Yalçın, K. Aslantaş, A. Erçetin, Comparative analysis of minimum chip thickness, surface quality and burr formation in micro-milling of wrought and selective laser melted Ti64, Micromachines 14 (6) (Jun. 2023), https://doi.org/10.3390/mi14061160.

[11] R. Messing, M. Kloker, Smart suction — an advanced concept for laminar flow control of three-dimensional boundary layers, in: M. Resch, S. Roller, P. Lammers, T. Furui, M. Galle, W. Bez (Eds.), High Performance Computing on Vector Systems 2007, Springer, Berlin, Heidelberg, 2008, pp. 53–60, https://doi.org/10.1007/978-3-540-74384-2_6.

[12] J. Xu, A review on tool wear issues in drilling CFRP laminates, Front. Mater. 9 (Sep) (2022), https://doi.org/10.3389/fmats.2022.990773.

[13] T. Chen, J. Liu, C. Li, J. Zhang, G. Wang, M. Li, Study on tool wear and cutting performance of CFRP for inclined angle milling, Int. J. Adv. Manuf. Technol. 129 (9) (Dec. 2023) 3933–3947, https://doi.org/10.1007/s00170-023-12558-9.

[14] Y. Bai, et al., A semi-analytical model for predicting tool wear progression in drilling CFRP, Wear 486–487 (Dec. 2021) 204119, https://doi.org/10.1016/j.wear.2021.204119.

[15] G. Czél, M. Jalalvand, M.R. Wisnom, T. Czigány, Design and characterisation of high performance, pseudo-ductile all-carbon/epoxy unidirectional hybrid composites, Compos. B Eng. 111 (Feb. 2017) 348–356, https://doi.org/10.1016/j.compositesb.2016.11.049.

[16] S. Li, et al., Formation mechanism of outlet damage in interlaminar drilling of CFRP, Int. J. Adv. Manuf. Technol. 129 (11) (Dec. 2023) 5117–5133, https://doi.org/10.1007/s00170-023-12643-z.

[17] S. Gaugel, et al., A comparative study on tool wear and laminate damage in drilling of carbon-fiber reinforced polymers (CFRP), Compos. Struct. 155 (Nov. 2016) 173–183, https://doi.org/10.1016/j.compstruct.2016.08.004.

[18] Y. Karpat, O. Bahtiyar, Tool geometry based prediction of critical thrust force while drilling carbon fiber reinforced polymers, Adv. Manuf. 3 (4) (Dec. 2015) 300–308, https://doi.org/10.1007/s40436-015-0129-y.

[19] R.S. Anand, K. Patra, Mechanistic cutting force modelling for micro-drilling of CFRP composite laminates, CIRP Journal of Manufacturing Science and Technology 16 (Jan. 2017) 55–63, https://doi.org/10.1016/j.cirpj.2016.07.002.

[20] B. Yalçın, A. Yüksel, K. Aslantaş, O. Der, A. Ercetin, Optimization of micro-drilling of laminated aluminum composite panel (Al–pe) using taguchi orthogonal array design, Materials 16 (13) (Jan. 2023), https://doi.org/10.3390/ma16134528. Art. no. 13.

[21] A. Dogrusadik, A. Kentli, Experimental investigation of support plates' influences on tool wear in micro-drilling of CFRP laminates, J. Manuf. Process. 38 (Feb. 2019) 214–222, https://doi.org/10.1016/j.jmapro.2019.01.018.

[22] X. Wang, P.Y. Kwon, C. Sturtevant, D, Dae-W. Kim, J. Lantrip, Tool wear of coated drills in drilling CFRP, J. Manuf. Process. 15 (1) (Jan. 2013) 127–135, https://doi.org/10.1016/j.jmapro.2012.09.019.

[23] I.S. Shyha, D.K. Aspinwall, S.L. Soo, S. Bradley, Drill geometry and operating effects when cutting small diameter holes in CFRP, Int. J. Mach. Tool Manufact. 49 (12) (Oct. 2009) 1008–1014, https://doi.org/10.1016/j.ijmachtools.2009.05.009.

[24] B.Z. Balázs, N. Geier, M. Takács, J.P. Davim, A review on micro-milling: recent advances and future trends, Int. J. Adv. Manuf. Technol. 112 (3) (Jan. 2021) 655–684, https://doi.org/10.1007/s00170-020-06445-w.

[25] M. Perçin, K. Aslantas, İ. Ucun, Y. Kaynak, A. Çicek, Micro-drilling of Ti–6Al–4V alloy: the effects of cooling/lubricating, Precis. Eng. 45 (Jul. 2016) 450–462, https://doi.org/10.1016/j.precisioneng.2016.02.015.

[26] J.W. Kim, J. Nam, J. Jeon, S.W. Lee, A study on machining performances of micro-drilling of multi-directional carbon fiber reinforced plastic (MD-CFRP) based on nano-solid dry lubrication using graphene NanoPlatelets, Materials 14 (3) (Jan. 2021), https://doi.org/10.3390/ma14030685.

[27] H. Inoue, et al., Influence of tool wear on internal damage in small diameter drilling in GFRP, Compos. Struct. 39 (1) (Sep. 1997) 55–62, https://doi.org/10.1016/S0263-8223(97)00068-8.

[28] A. Faraz, D. Biermann, K. Weinert, Cutting edge rounding: an innovative tool wear criterion in drilling CFRP composite laminates, Int. J. Mach. Tool Manufact. 49 (15) (Dec. 2009) 1185–1196, https://doi.org/10.1016/j.ijmachtools.2009.08.002.

[29] N. Geier, Egyirányban szénszállal erősített polimer (UD-CFRP) kompozit anyagok forgácsolt alaksajátosságainak mikro- és makrogeometriai vizsgálata és jellemző mérőszámrendszerének kidolgozása. Analysis of Machining Induced Micro- and Macro-Geometrical Damages of Unidirectional Carbon Fibre Reinforced Polymer (UD-CFRP) Composites, and the Development of its Characteristics Measures, 2019. https://repozitorium.omikk.bme.hu/handle/10890/13185.

[30] F. Wang, B. Qian, Z. Jia, R. Fu, D. Cheng, Secondary cutting edge wear of one-shot drill bit in drilling CFRP and its impact on hole quality, Compos. Struct. 178 (Oct. 2017) 341–352, https://doi.org/10.1016/j.compstruct.2017.04.024.

[31] E. Pliusys, P.T. Mativenga, Reducing delamination in micro drilling of carbon composite materials, in: S. Hinduja, P.J. da Silva Bartolo, L. Li, W.-Y. Jywe (Eds.), Proceedings of the 38th International MATADOR Conference, Springer International Publishing, Cham, 2022, pp. 337–356, https://doi.org/10.1007/978-3-319-64943-6_24.

[32] J.W. Kim, J. Nam, S.W. Lee, Experimental study on micro-drilling of unidirectional carbon fiber reinforced plastic (UD-CFRP) composite using nano-solid lubrication, J. Manuf. Process. 43 (Jul. 2019) 46–53, https://doi.org/10.1016/j.jmapro.2019.04.022.

[33] M. Slamani, J.-F. Chatelain, H. Hamedanianpour, Comparison of two models for predicting tool wear and cutting force components during high speed trimming of CFRP, Int J Mater Form 8 (2) (Apr. 2015) 305–316, https://doi.org/10.1007/s12289-014-1170-2.

[34] L.L. Alhadeff, M.B. Marshall, D.T. Curtis, T. Slatter, Protocol for tool wear measurement in micro-milling, Wear 420 (421) (Feb. 2019) 54–67, https://doi.org/10.1016/j.wear.2018.11.018.

[35] G. Yu, C. Li, J. Sun, Machine fault diagnosis based on Gaussian mixture model and its application, Int. J. Adv. Manuf. Technol. 48 (1) (Apr. 2010) 205–212, https://doi.org/10.1007/s00170-009-2283-5.

[36] C. Pereszlai, N. Geier, Comparative analysis of wobble milling, helical milling and conventional drilling of CFRPs, Int. J. Adv. Manuf. Technol. 106 (9) (Feb. 2020) 3913–3930, https://doi.org/10.1007/s00170-019-04842-4.

[37] D.I. Poór, N. Geier, C. Pereszlai, J. Xu, A critical review of the drilling of CFRP composites: burr formation, characterisation and challenges, Compos. B Eng. 223 (Oct. 2021) 109155, https://doi.org/10.1016/j.compositesb.2021.109155.

[38] D. Geng, et al., Delamination formation, evaluation and suppression during drilling of composite laminates: a review, Compos. Struct. 216 (May 2019) 168–186, https://doi.org/10.1016/j.compstruct.2019.02.099.